JOURNAL OF MODERN OPTICS, 2002,
VOL. 49, NO. 14/15, 2423–2435

Taylor & Francis
Taylor & Francis Group

Metal coverage dependence of local optical properties of semicontinuous metallic films

KATYAYANI SEAL, MARK A. NELSON† and Z. CHARLES YING

Department of Physics, New Mexico State University, Las Cruces, New Mexico 88003-8001, USA

DENTCHO A. GENOV, ANDREY K. SARYCHEV and VLADIMIR M. SHALAEV

School of Electrical and Computer Engineering, Purdue University, West Lafayette, Indiana 47907-1285, USA

(*Received 15 February 2002; revision received 17 April 2002*)

Abstract. Semicontinuous silver films on insulator substrates, which exhibit unique electrical and optical properties, were studied experimentally and theoretically. The percolation threshold of the films, which were synthesized by laser ablation, was determined from a combination of studies of the surface morphology by electron microscopy and the dc electrical resistance as a function of metal concentration. Local optical properties measured by near-field optical microscopy were compared with theoretical results obtained using the Block elimination method, with good agreement. Local field distributions were found to depend on the metal concentration and wavelength of illumination. The degree of localization was found to increase at metal concentrations above and below the percolation threshold.

1. Introduction

Nanoscaled semicontinuous metallic structures (or random metal–dielectric composites) have been an area of great interest over the past few years on account of their unique optical and electrical transport properties, which are notably different from those of their corresponding bulk counterparts [1–18]. One of the most remarkable properties of such composite systems is the localization and enhancement of electric and magnetic fields at visible and infrared frequencies [6–8]. These materials show promise in applications such as broad-band optical amplifiers, single molecular spectroscopy [19] and optical limiters [20]. This paper reports systematic experimental analysis of the changes in the local optical properties and electrical conductivity with metal concentration and corroborates it with theoretical models.

Metal–dielectric composites are typically synthesized by deposition of metal particles on to a dielectric substrate [21, 22]. At low metal concentrations, mutually

† Also at Department of Chemical Engineering, New Mexico State University, Las Cruces, New Mexico 88003-8001, USA.

Journal of Modern Optics ISSN 0950-0340 print/ISSN 1362-3044 online © 2002 Taylor & Francis Ltd
http://www.tandf.co.uk/journals
DOI: 10.1080/0950034021000011482

separated nanometre-sized grains are formed on the substrate. Self-similar clusters form as the metal concentration (filling fraction) increases. The geometrical properties of these nanostructures, for example the scale invariance or fractality of the clusters, play an important role in determining the physical properties of these systems [1–3, 6–8]. At a metal concentration called the percolation threshold p_c, initially separated clusters interconnect to form an infinite cluster of metal, enabling a continuous current path in the system. The percolation threshold marks an insulator-to-metal phase transition and is accompanied by a sharp drop in dc resistivity [9] and anomalous absorption at visible and near-infrared wavelengths [1]. At even higher metal concentrations, the sample becomes mostly metallic with dielectric voids, ultimately resulting in a uniform metal film.

The unique geometrical properties of metal–dielectric composites lead to localization of surface plasmons, an effect related to Anderson localization [1, 2]. As a result, electromagnetic energy is also concentrated in nanosized areas (called hot spots) where electric and magnetic fields are strongly enhanced. These localized electromagnetic field fluctuations in metal–dielectric systems are especially prominent at optical and near-infrared wavelengths where the resulting local fields can exceed the incident field by up to 10^5 for the linear and up to 10^{20} for the nonlinear optical responses, such as four-wave mixing [1–3]. This phenomenon was predicted by scaling theory [1, 6] and has been verified in numerical calculations using the exact block elimination [10] and non-exact real-space renormalization group procedures [1, 7]. The spatial locations of the field maxima depend on the polarization, wavelength and angle of incidence of the applied field [16]. The distribution (both separation and magnitude) of the local field is also expected to vary with metal concentration, a phenomenon that has not been experimentally investigated in the past.

In the present paper, we have experimentally studied the changes in electrical resistivity and the local field distribution with metal concentration (filling fraction) and compared them with the results obtained from theoretical calculations based on an exact numerical method (block elimination method) for two different wavelengths. Near-field scanning optical microscopy (NSOM) provides subwavelength optical resolution and is ideally suited to investigate experimentally the local field distributions of these composites in the optical and near-infrared spectral ranges. Full correlation between theoretical and experimental distributions has been observed.

In section 2, details of the experiment are described while section 3 briefly covers the theoretical calculations and the averaging methods used in our studies. In section 4 both the experimental and the theoretical results are presented and discussed. Conclusions are provided in section 5.

2. Experiment

The samples of random metal–dielectric films used in our experiments were synthesized by laser ablation of a solid silver target under an argon gas pressure of 0.3 mTorr. Laser pulses with an energy of 100 mJ pulse^{-1}, a repetition rate of 10 Hz and a wavelength of 532 nm were provided by a neodymium-doped yttrium aluminium garnet laser (Quanta-Ray DCR-02A). The spot size of the laser beam at the target was approximately 1 mm^2. Glass substrates for NSOM study, Formvar-coated copper grids for characterization by transmission electron

microscopy (TEM) and silicon substrates for scanning electron microscopy (SEM) analysis were placed horizontally at a predetermined distance from the target.

The electrical resistance of the samples was measured *in situ* using an electrometer (Keithley 610C). Optical transmittance and reflectance measurements were also carried out *in situ* by having a diode laser (Melles Griot 06-DAL-103) operating at 650 nm provide the incident beam and using power meters (Newport 1830C) to measure the power of the transmitted and reflected beams. The resulting absorption profile was obtained with increasing metal concentration and helped to mark the percolation threshold concentration.

The microstructure of the samples was studied by electron microscopy. A transmission electron microscope (Hitachi H-7000) was used to study the silver films deposited on Formvar-coated copper grids, a type of TEM substrate. The filling fraction was calculated for each transmission electron micrograph by using image-processing techniques. The glass substrate used for NSOM is not suitable for electron microscopy measurements because of its large thickness and low electrical conductivity. In order to investigate possible differences in morphologies of the silver films deposited on glass and deposited on Formvar, additional studies were carried out using a scanning electron microscope (Hitachi S-800) with a field emission gun for samples of silver films deposited on substrates of semiconductor silicon and Formvar-coated copper grids. The surface of silicon has a native SiO_2 layer, which serves as a good representation of the SiO_2 glass substrate used for NSOM. The SEM results indicate qualitatively similar morphologies for the silver films deposited on SiO_2 and Formvar.

The silver–glass samples with different metal concentrations were analysed with a near-field scanning optical microscope (Quesant Q250). Samples were mounted on the hypotenuse face of a BK7 glass prism with index-matching fluid and illuminated by the evanescent field in the total-internal-reflection geometry at an incident angle $\theta = 47°$. The illumination sources were helium-neon lasers operating at wavelengths of 543 and 633 nm. The local optical signal was collected by a tapered uncoated optical fibre with a tip radius of about 50 nm and fed to a photomultiplier tube. A fibre puller (Sutter Instruments P-2000) was used to taper the optical fibre.

During NSOM experiments, the tip–sample separation was maintained at a distance $h \approx 10$ nm by using non-optical shear-force feedback [23]. All NSOM data were normalized with respect to the intensity of the evanescent field, which was obtained by measuring the average intensity value for a clear glass substrate. It was ensured that the evanescent field, when measured at a height h above the sample surface (tip–sample separation is about h), does not decay significantly compared with the evanescent field at the sample surface ($h = 0$) by using the formula

$$I_{\text{measured}} = I_0 \exp\left(-\frac{2\pi h[(n\sin\theta)^2 - 1]^{1/2}}{\lambda}\right), \tag{1}$$

where λ is the light wavelength in vacuum and $n \approx 1.5$ is the index of refraction of the glass substrate. At a height of 10 nm, the signal loss is only about 4.5%.

3. Numerical calculations and theory

The theoretical approach for treating the existence of high-order local field enhancement in percolation systems was established just recently [4–8]. As shown by the Sarychev–Shalaev theory, for the special case of surface plasmon resonance at $\varepsilon_d = -\mathrm{Re}\,(\varepsilon_m)$ (where ε_m and ε_d are the dielectric functions of the metallic and dielectric components respectively), the problem of the field potential distribution across the sample can be mapped to the Anderson transition problem. The localization and optical properties at $|\varepsilon_m/\varepsilon_d| \gg 1$ can be found by the scale renormalization developed in [4–8]. The predicted localization phenomenon has been verified experimentally [11] and numerically by using an approximate numerical scheme [7] and later with an exact block elimination procedure [10]. It was found that, in the vicinity of the percolation threshold p_c, the local field has a very wide log-normal distribution which transforms into a power-law distribution away from p_c. Similar power-law distributions were found theoretically for fractal aggregates [12] whereas, in the case of the metal–dielectric composites, the exponent was close to the 'single-dipole' value of 1.5. Experimental studies on the intensity distribution in nanostructured surfaces were performed in [17]. However, until now the intensity distributions in metal–dielectric films at the percolation threshold have never been studied.

Numerical calculations based on the block elimination method, which has been described in detail elsewhere [10], were used to calculate the local field distribution for silver–glass composite films at wavelengths of 543 and 633 nm to coincide with the wavelengths used in our experimental studies. The images were then averaged over an area corresponding to the resolution limit of the experimental data (120 nm × 120 nm). This resolution limit was arrived at by measuring the full width at half-maximum for various peaks in the experimental images. The field vectors are symmetrically distributed about zero with positive and negative values. The averaging process leads to destructive interference and, as a result, the mean field strength diminishes rapidly. In order to compare theoretical and experimental data, we averaged over an area (corresponding to the resolution limit of the microscope) where approximately 50 local field peaks are situated.

The numerical process for creating silver–glass structures involves random incidence of silver particles on to a glass substrate. A straightforward probability relation that connects surface filling fraction $p(t)$ as a function of the time of deposition can be used to describe this process. It should be noted that surface diffusion is not accounted for in this model. Assuming that the metal particles fall individually on the substrate, a recurrence relation can be written for the surface area S_n covered after the nth particle reaches the film:

$$S_n = (S_{n-1} + S_0)(1 - P) + S_{n-1}P,$$

where $P = S_{n-1}/S_{\mathrm{total}}$ is the probability for the nth particle to fall over an area already covered by metal while S_{total} and S_0 are the total surface area of the film and the size of a single particle respectively. The solution of this recurrence relation can be found in terms of the surface filling fraction

$$p(t) = 1 - b^t, \tag{2}$$

where t is the deposition time and the coefficient $b = 1 - S_0/S_{\mathrm{total}} = 2^{-1/t_c}$ is obtained from the time t_c required to reach the percolation threshold $p = p_c$. Using equation (2) and the effective-medium approximation [9] to calculate the

effective resistance ρ_{eff} as a function of surface coverage, we obtain the known result

$$\rho_{\text{eff}} \sim \begin{cases} \rho_{\text{m}}(p - p_{\text{c}})^{-r}, & \begin{cases} 0 < p - p_{\text{c}} \ll 1, \\ 0 < p_{\text{c}} - p \ll 1, \end{cases} \\ \rho_{\text{d}}(p_{\text{c}} - p)^{s}, \end{cases} \tag{3}$$

where ρ_{m} and ρ_{d} are constants. A correlation can be established between parameters in the experimental and numerical methods. Below we use the values (corresponding to the two-dimensional model) $s = r = 1.3$ for the critical exponents [9].

4. Results and discussion

4.1. *Morphology and electrical resistance*

Figure 1 shows a series of transmission electron micrographs of silver–Formvar films with different laser ablation time durations of 10, 20, 30 and 40 min. The four images, each 1000 nm × 1000 nm in size, were recorded at the same magnification. The dark features in these images represent silver. The filling fraction (surface coverage) p, defined as the percentage of area covered by the silver grains, is

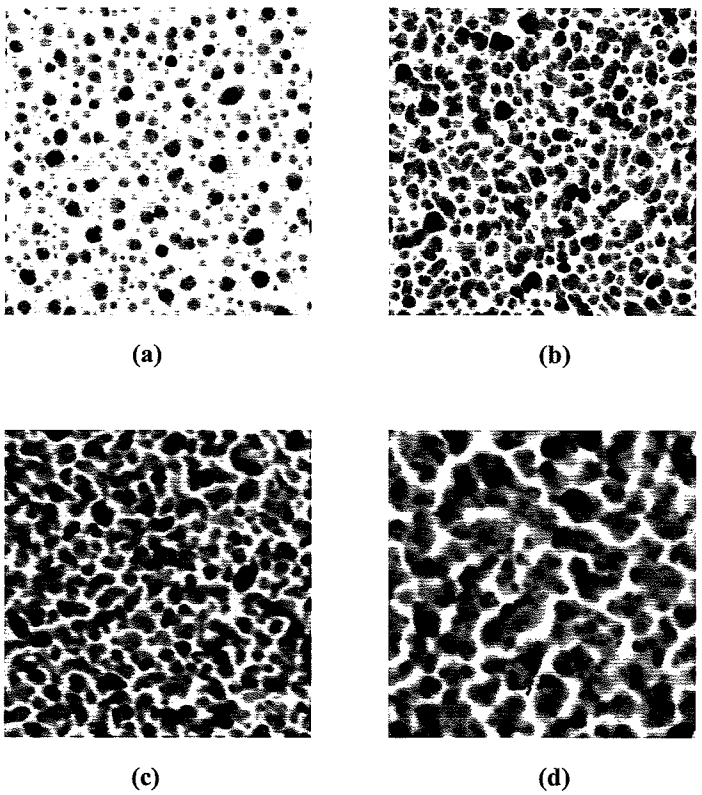

Figure 1. TEM images (1 μm × 1 μm) of silver films at various metal concentrations p corresponding to different deposition times t showing a transition from individual metal grains to interconnected clusters: (*a*) $t = 10$ min; (*b*) $t = 20$ min; (*c*) $t = 30$ min; (*d*) $t = 40$ min. The filling fractions are given in table 1.

Table 1. Metal filling fraction and electrical resistance of the films deposited at different deposition times.

Deposition time t (min)	Filling fraction p	Electrical resistance (Ω)
10	0.36	1.0×10^{12}
20	0.45	5.0×10^{10}
30	0.65	3.0×10^{8}
40	0.73	1.0×10^{8}

calculated from each image. In order to compute the filling fraction, the raw TEM images in grey scale were processed and a threshold value for brightness was selected. Above this threshold, a pixel would record as a bright spot (with a value of 1) and below it, as a dark spot (with a value of 0). The numbers of 1s and 0s were counted to measure the area covered by silver and the area left bare respectively. The results are summarized in table 1. The transition from individual metal grains to isolated metal clusters and then to interconnected clusters with increase in laser ablation time and the filling fraction can be seen clearly in figure 1. Individually separated metal grains are seen in figure 1 (*a*) with an average grain size of about 15 nm. For the sample corresponding to figure 1 (*b*) the filling fraction increases to about $p = 0.45$, which is close to the theoretically predicted percolation threshold value of 0.5 [10] and the beginning of cluster formation is evident. With further increase in p, figure 1 (*c*) shows interconnected clusters of silver at a value of $p = 0.62$, which is somewhat beyond the percolation threshold. Figure 1 (*d*) exhibits mostly metal with small dielectric voids and at a value of $p = 0.8$, is significantly beyond the percolation threshold.

Theoretically simulated images of the morphology of silver particles on a dielectric substrate are shown in figures 2 (*a*), (*b*) and (*c*) at filling fractions of 0.3, 0.5 and 0.7 respectively. The images are 1000 nm × 1000 nm in size. Similar to the TEM images in figure 1, silver is indicated by dark features. The average grain size in all three images is about 20 nm. Figure 2 (*a*), at a filling fraction of 0.3, is below the percolation threshold and shows individually separated grains as well as some

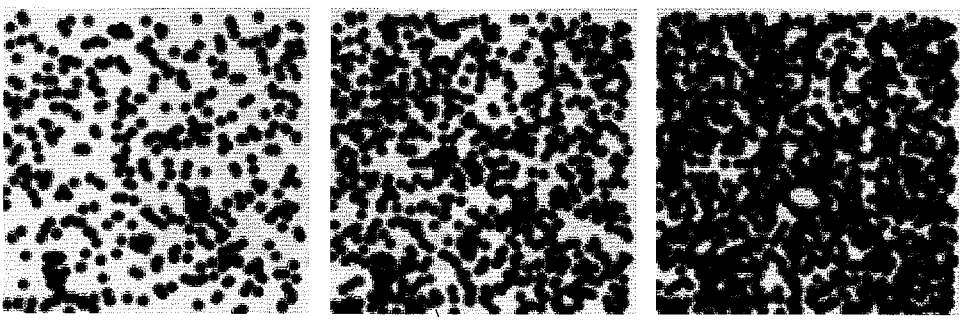

(a) **(b)** **(c)**

Figure 2. Theoretically simulated images (1 μm × 1 μm) of silver films at various metal concentrations p: (*a*) $p = 0.3$; (*b*) $p = 0.5$; (*c*) $p = 0.7$.

clusters at the initial stages of their formation. Figure 2 (*b*), at a filling factor of 0.5, is at the percolation threshold and shows the existence of large interconnected clusters with very few individual grains. Figure 2 (*c*), at a filling factor of 0.7, is well above the percolation threshold and shows the existence of dielectric voids in a primarily metal film. Figures 1 and 2 indicate a fairly good correspondence between experimentally synthesized samples and theoretically simulated images. The variation in metal particle size in actual experiments has been studied elsewhere and was found to follow a wide log-normal distribution [24]. The effect of this on the local field intensities and other phenomenon is a subject of future study.

The dependence of filling fraction on deposition time is shown in figure 3. The experimental data are represented by symbols. The fact that some amount of image processing is required while calculating the filling fractions in order to obtain a contrast large enough to distinguish between dark and bright pixels in the images contributes to the error bars in the experimental data. The difference in substrate properties between glass (for optical and electrical measurements) and Formvar (for the TEM measurements) also contributes to the error in experimental filling fraction estimates. The three theoretical curves are obtained from equation (2) at three different values of the parameter b corresponding to three values of deposition time (20, 25 and 30 min) when a film reaches the percolation threshold. Within the error margins, the experimental data fit best for the theoretical curve with p_c set at a deposition time of 20 min. The curves with p_c set at 25 and 30 min are progressively further from the experimental data. However, all three theoretical curves follow the same trend and agree reasonably well with the experiment.

The resistance versus filling fraction curve (figure 4) dips sharply between filling fraction values of 0.4 and 0.7 with the midpoint of the drop being at about $p = 0.5$. The theoretical curve was obtained from equation (3) by setting $\rho_d \approx 10^{14}\,\Omega$ (the experimentally measured value for a pure glass substrate) and $\rho_m \approx 10^7\,\Omega$ (the experimentally measured value for a mostly metal film). The experiment involved the measurement of electrical resistance with increasing

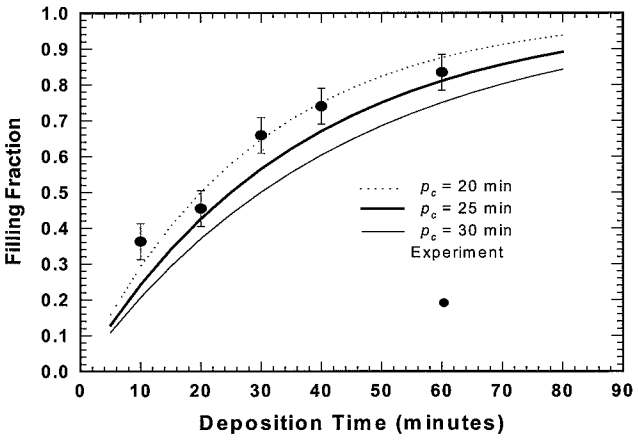

Figure 3. Filling fraction p versus deposition time t. The theoretical curves are calculated using equation (2) with p_c set at three different deposition times of 20, 25 and 30 min.

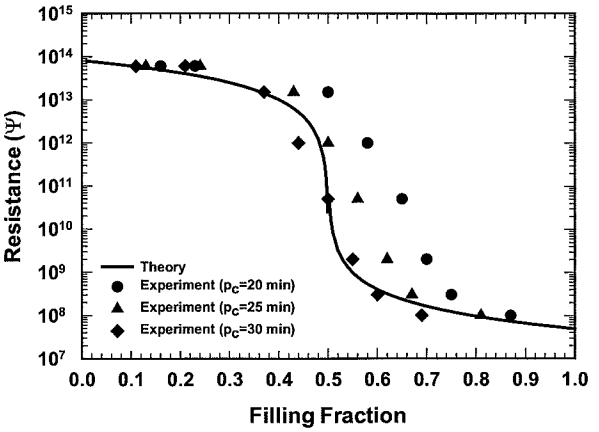

Figure 4. Resistance versus filling fraction. The filling fraction data are obtained from the theoretical curves in figure 3. The corresponding resistance values for each theoretical line in figure 3 is indicated by the symbols.

values of deposition time t. The deposition times were then correlated to the corresponding filling fraction value p obtained from the theoretical curves in figure 3. There are thus three sets of experimental data corresponding to the three theoretical curves in figure 3. Of the three, the best match between theory and experiment is for the data with p_c set at 30 min. Based on the results described in figures 3 and 4, we concluded that percolation occurs at a deposition time between 20 and 30 min (between $p = 0.45$ and $p = 0.62$) for the experimental conditions used in our set-up.

4.2. *Near-field optical properties at the percolation threshold*

Figures 5 and 6 pertain to the local optical properties of samples with different metal concentrations: at $p \approx p_c$ (figure 5) and at $p < p_c$ and $p > p_c$ (figure 6).

Figure 5 (*a*) exhibits near-field intensity profiles experimentally recorded over a $4\,\mu m \times 4\,\mu m$ area for a sample near the percolation threshold ($t = 20$ min and $p = 0.45$). The illumination wavelength is 543 nm. The image exhibits a very non-uniform distribution of near-field optical intensity with peak intensities reaching values as high as 20 times the intensity of the incident evanescent wave.

Theoretically calculated near-field optical intensity profiles of a film at the percolation threshold with filling fraction $p = p_c = 0.5$, with and without averaging, are shown in figures 5 (*b*) and (*c*) respectively. The averaging process was carried out in order to compare theory effectively with experiment, the latter being limited by the resolution of the near-field scanning optical microscope (120 nm). The resulting averaged theoretical distribution is shown in figure 5 (*b*). The experimental data (figure 5 (*a*)) and the theoretically computed result after the averaging process (figure 5 (*b*)) closely resemble each other. They have similar general features and about the same peak enhancement factors of 20–30. It should be emphasized, however, that the exact distributions of the near-field optical intensity, such as the exact peak positions, in these two images should not be compared because the films used for the experimental studies and theoretical calculations have different arrangements of the metal clusters.

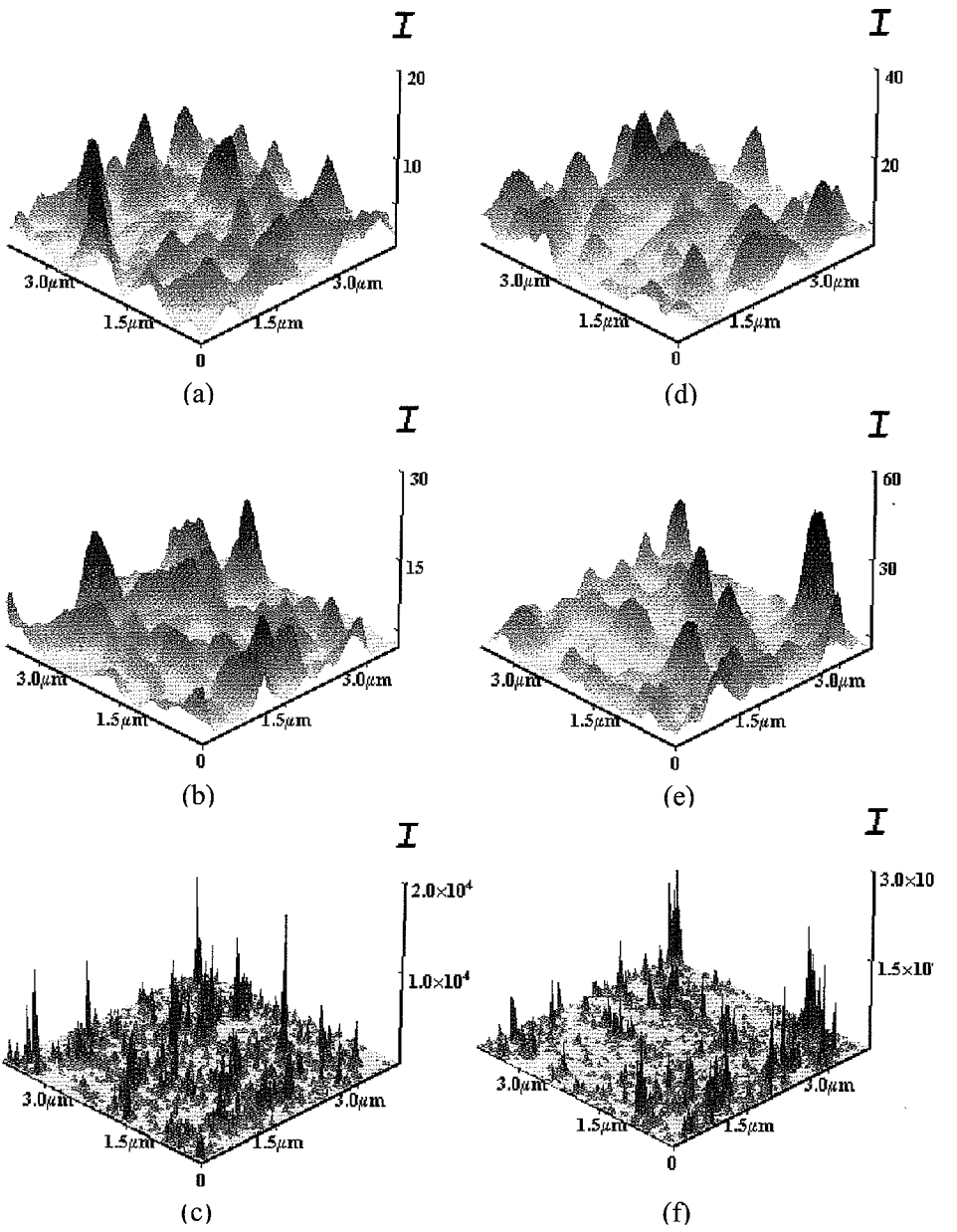

Figure 5. (*a*), (*d*) Experimental (NSOM), (*b*), (*e*) averaged theoretical and (*c*), (*f*) raw theoretical optical intensity images over a 4 μm × 4 μm area for $p \approx p_c$ at illumination wavelengths λ of (*a*)–(*c*) 543 nm and (*d*)–(*f*) 633 nm.

In figure 5 (*c*), which shows the theoretical local field intensity over a 4 μm × 4 μm area, the optical feature sizes are comparable with the particle sizes in the sample (about 15 nm). The image consists of a large number of highly intense localized peaks (hot spots) spread over the sample. The values for the maximum enhancement factors in these peaks are extremely high (up to about

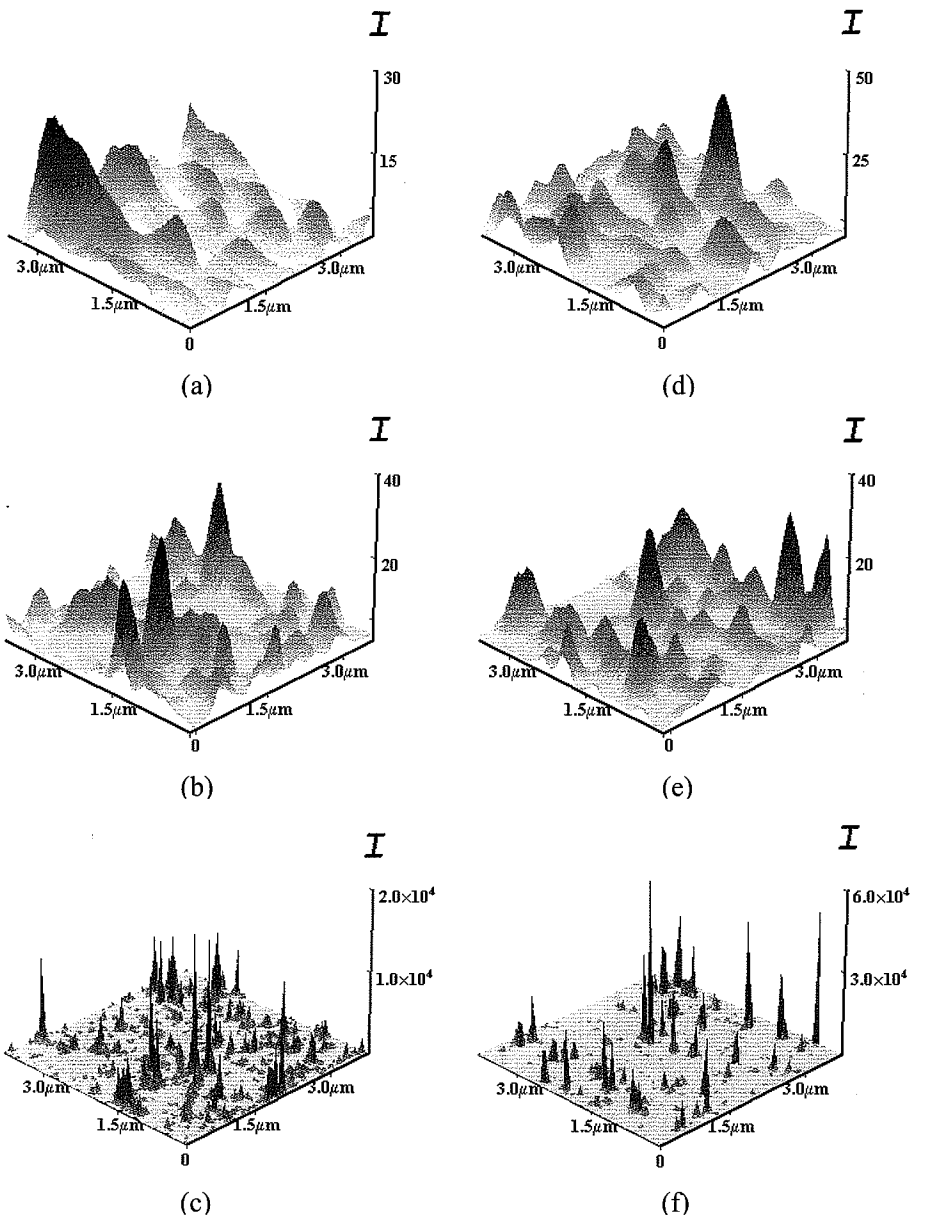

Figure 6. (*a*), (*d*) Experimental (NSOM), (*b*), (*e*) averaged theoretical and (*c*), (*f*) raw theoretical optical intensity images over a $4 \times 4\,\mu\text{m}$ area at $\lambda = 633\,\text{nm}$ for (*a*)–(*c*) $p < p_c$ and (*d*)–(*f*) $p > p_c$.

10^4). Although not evident in figures 5 (*a*) and (*b*), where the absolute value squared of the local fields is shown (the applied field is assumed to have a magnitude of one), it is important to note that the local field vectors are distributed uniformly about zero with comparable numbers of positive and negative values. On comparing figures 5 (*a*) and (*b*) with figure 5 (*c*), it is evident that there is a significant drop in the field intensities in the former, an effect that is due to

destructive interference and the mutual cancellation of the field vectors during the averaging process. There is, however, a degree of preservation of large-scale local field topology in figure 5 (*b*) in that the majority of high-intensity local field features (groups or 'clumps' of peaks which are in spatial proximity) seen in figure 5 (*c*) are generally preserved in figure 5 (*b*) as well.

Figure 5 (*d*) represents the experimentally obtained near-field intensity profile over the same 4 μm × 4 μm area of the sample used for figure 5 (*a*) ($t = 20$ min and $p = 0.45$) at an illumination wavelength of 633 nm. Figures 5 (*e*) and 5 (*f*) are the corresponding theoretical calculations, with and without averaging respectively. The averaging process results in the same effects of increase in feature size and decrease in peak intensities as described for figures 5 (*a*), (*b*) and (*c*). These images again exhibit a very non-uniform distribution of near-field optical intensity with peak intensities reaching values as high as 40 times the incident intensities for figures 5 (*d*) and (*e*) and 10^4 times the incident intensity for figure 5(*f*).

It is important to note that the average enhancement factors increase with increasing wavelength, as is evident on comparing images from the two wavelengths in figure 5. This wavelength dependence of the average local field has been predicted by scaling theory [6]. It should also be noted that the exact locations of peaks depend on the wavelength of illumination.

4.3. *Below and above the percolation threshold*

Figures 6 (*a*), (*b*) and (*c*) are the experimental, averaged theoretical and raw theoretical images respectively over a 4 μm × 4 μm area at a metal concentration ($p = 0.3$) less than the percolation threshold. Figures 6 (*d*), (*e*) and (*f*) are the corresponding images above the threshold at $p = 0.7$. The averaged theoretical images have again been calculated by the method described earlier and show the same large-scale correspondence with the experimental NSOM images. Again, the NSOM images show a highly non-uniform distribution of local optical intensity with peak intensities reaching values as high as 30 times the intensity of the incident wave. However, on comparing figure 5 (*d*) with figures 6 (*a*) and (*d*), all recorded at a wavelength of 633 nm, it is evident that the density of intensity peaks is smaller in the latter cases. Thus, at both $p < p_c$ and $p > p_c$, the distance between the intensity peaks is larger in comparison with the distances at $p = p_c$, which indicates stronger localization at both $p < p_c$ and $p > p_c$. This is also seen on comparing the corresponding averaged theoretical (figure 5 (*e*) with figures 6 (*b*) and (*e*)) and raw theoretical images (figure 5 (*f*) with figures 6 (*c*) and (*f*)). In all these cases, the enhancement factors of individual peaks are higher than that observed at $p = p_c$, but the number of peaks is smaller in comparison. We can conclude that these properties of the field distribution are preserved on larger scales as well. The theoretically predicted increase in localization and magnitude of enhancement in individual hot spots when the surface coverage fractions depart from the percolation threshold value appears to be confirmed by experiment as well.

5. Conclusions

A study of the surface morphology (by TEM), dc electrical properties (via resistance measurements), and local optical properties (by NSOM) of silver films deposited by laser ablation with various metal concentrations was carried out and

compared with the results obtained from theoretical modelling. Based on the morphology and filling fraction values, it is evident that the percolation threshold in these metal–dielectric composites occurred at a deposition time between 20 and 30 min for the deposition conditions used. This is further confirmed by the sharp drop in resistance (by a factor of 10^3) in this time period. The experimental filling fraction and resistance data agree reasonably well with those from the theoretical models. The NSOM images obtained show strong enhancement of the local fields through the existence of hot spots with high intensities. For local optical studies, comparison between experimental data and a numerical model based on the block elimination method has been made. For both theory and experiment, the optical enhancement observed at the percolation threshold is quite different from that observed at higher and lower metal concentrations, where stronger localization and an increase in individual peak intensities are observed. It was also observed that both the localization and the intensities of the hot spots depend on the incident wavelength.

Acknowledgments

The project is supported in part by the Army Research Office (grant DAAD19-01-1-0682), National Aeronautics and Space Administration (grant NAG8-1710), National Science Foundation (grant DMR0121814) and New Mexico Universities Collaborative Research Program at Los Alamos National Laboratory. The authors acknowledge technical assistance provided by Dr S. Ghoshroy, Dr L. Trillo, Mr M. Barela and Dr. R. Liefeld and experimental assistance provided by D. Smirnova.

References

[1] Shalaev, V. M., 2000, *Nonlinear Optics Of Random Media: Fractal Composites and Metal-Dielectric Films* (Berlin: Springer).
[2] Stauer, D., and Aharony, A., 1991, *Introduction to Percolation Theory*, Second edition (London: Taylor & Francis).
[3] Sarychev, A. K., and Shalaev, V. M., 2000, *Optics of Nanostructured Materials*, edited by V. A. Markel and T. F. George (New York: Wiley).
[4] Sarychev, A. K., and Shalaev, V. M., 2000, *Phys. Rep.*, **335,** 275.
[5] Shubin, V. A., Sarychev, A. K., Clerc, J. P., and Shalaev, V. M., 2000, *Phys. Rev.* B, **62,** 11 230.
[6] Sarychev, A. K., and Shalaev, V. M. , 2002, *Optical Properties of Nanostructured Random Media*, Topics in Applied Physics, Vol. 82, Edited by V. M. Shalaev (Berlin: Springer) pp. 169–184.
[7] Shalaev, V. M., and Sarychev, A. K., 1998, *Phys. Rev.* B, **57,** 13 265.
[8] Sarychev, A. K., Shubin, V. A., and Shalaev, V. M., 1999, *Phys. Rev.* B, **60,** 16 389.
[9] Bergman, D. J., and Stroud, D., 1992, *Solid St. Phys.*, **46,** 147.
[10] Genov, D. A., Sarychev, A. K., and Shalaev, V. M., 2002 (submitted).
[11] Gresillin, S. *et al*, 1999, *Phys. Rev. Lett.*, **82,** 4520.
[12] Stockman, M. I., Pandey, L. N., Muratov, L. S., and George, T. F., 1994, *Phys. Rev. Lett.*, **72,** 2486.
[13] Brouers, F., Blacher, S., Lagarov, A. N., Sarychev, A. K., Gadenne, P., and Shalaev, V. M., 1997, *Phys. Rev.* B, **55,** 13 234; Gadenne, P., Brouers, F., Shalaev, V. M., and Sarychev, A. K., 1998, *J. Opt. Soc. Am.* B, **15,** 68; Sarychev, A. K., and Shalaev, V. M., 1999, *Physica* A, **266,** 115; Sarychev, A. K., Shubin, V. A., and Shalaev, V. M., 1999, *Phys. Rev.* E, **59,** 7239.

[14] DUCOURTIEUX, S., GRESILLON, S., BOCCARA, A. C., RIVOAL, J. C., QUELIN, X., GADENNE, P., DRACEHV, V. P., BRAGG, W. D., SAFONOV, V. P., PODOLSKIY, V. A., YING, Z. C., ARMSTRONG, R. L., and SHALAEV, V. M., 2000, *J. nonlinear opt. Phys. Mater.*, **9,** 105.

[15] SHALAEV, V. M., 1996, *Phys. Rep.* **272,** 61.

[16] DUCOURTIEUX, S., PODOSKIY, V. A., GRESILLON, S., BUIL, S., BERINI, B., GADENNE, P., BOCCARA, A. C., RIVOAL, J. C., BRAGG, W. D., BANERJEE, K., SAFONOV, V. P., DRACHEV, V. P., YING, Z. C., SARYCHEV, A. K., and SHALAEV, V. M., 2001, *Phys. Rev.* B., **64,** 165 403.

[17] BOZHEVOLNYI, S. I., and COELLO, V., 2001, *Phys. Rev.* B, **64,** 5414.

[18] BRAGG, W. D., MARKEL, V. A., KIM, W., BANERJEE, K., YOUNG, M. R., ZHU, J. G., ARMSTRONG, R. L., DANILOVA, Y. E., SAFONOV, V. P., SHALAEV, V. M., and YING, Z. C., 2001, *J. Opt. Soc. Am.* B, **18,** 698.

[19] KNEIPP, K., WANG, Y., KNEIPP, H., PERELMAN, L. T., ITZKAN, I., DASARI, R. R., and FELD, M. S., 1997, *Phys. Rev. Lett.*, **78,** 1667.

[20] CRANE, R., LEWIS, K., KHOSHNEVISAN, M., and VAN STRYLAND, E. (editors), 1995, *Materials for Optical Limiting, 1995* (Pittsburgh, Pennsylvania: Materials Research Society); HOOD, P., LEWIS, K., PACHTER, R., PERRY, J. W., HAGAN, D., and SUTHERLAND, R. (editors) 1997, *Materials for Optical Limiting II, 1997* (Pittsburgh, Pennsylvania: Materials Research Society).

[21] PLEKHANOV, A. I., PLOTNIKOV, G. L., and SAFONOV, V. P., 1991, *Opt. Spectrosc. (USSR)*, **71,** 451.

[22] OHRING, M., 1992, *The Materials Science of Thin Films* (San Diego, California: Academic Press).

[23] LEE, M., MCDANIEL, E. B., and HSU, J. W. P., 1996, *Rev. scient. Instrum.*, **67,** 1468.

[24] GRANQVIST, C. G., and HUNDERI, O., 1997, *Phys. Rev.* B, **16,** 3513.